Colloids and Surfaces B: Biointerfaces 129 (2015) 121–129

Contents lists available at ScienceDirect

Colloids and Surfaces B: Biointerfaces

journal homepage: www.elsevier.com/locate/colsurfb

Decompression induced bubble dynamics on ex vivo fat and muscle tissue surfaces with a new experimental set up

Virginie Papadopoulou[a,b,*], Sotiris Evgenidis[c], Robert J. Eckersley[d], Thodoris Mesimeris[e], Costantino Balestra[b,f], Margaritis Kostoglou[c], Meng-Xing Tang[a], Thodoris D. Karapantsios[c,**]

[a] Department of Bioengineering, Imperial College London, London, UK
[b] Environmental & Occupational Physiology Lab., Haute Ecole Paul Henri Spaak, Brussels, Belgium
[c] Department of Chemistry, Aristotle University of Thessaloniki, Thessaloniki, Greece
[d] Imaging Sciences & Biomedical Engineering Division, King's College London, London, UK
[e] Hyperbaric Department, St. Paul General Hospital of Thessaloniki, Thessaloniki, Greece
[f] DAN Europe Research Division, Belgium

ARTICLE INFO

Article history:
Received 15 December 2014
Received in revised form 17 February 2015
Accepted 10 March 2015
Available online 24 March 2015

Keywords:
Micronuclei
Nuclei
Decompression sickness
Degassing
Diving
Mass transfer

ABSTRACT

Vascular gas bubbles are routinely observed after scuba dives using ultrasound imaging, however the precise formation mechanism and site of these bubbles are still debated and growth from decompression in vivo has not been extensively studied, due in part to imaging difficulties. An experimental set-up was developed for optical recording of bubble growth and density on tissue surface area during hyperbaric decompression. Muscle and fat tissues (rabbits, ex vivo) were covered with nitrogen saturated distilled water and decompression experiments performed, from 3 to 0 bar, at a rate of 1 bar/min. Pictures were automatically acquired every 5 s from the start of the decompression for 1 h with a resolution of 1.75 μm. A custom MatLab analysis code implementing a circular Hough transform was written and shown to be able to track bubble growth sequences including bubble center, radius, contact line and contact angles over time. Bubble density, nucleation threshold and detachment size, as well as coalescence behavior, were shown significantly different for muscle and fat tissues surfaces, whereas growth rates after a critical size were governed by diffusion as expected. Heterogeneous nucleation was observed from preferential sites on the tissue substrate, where the bubbles grow, detach and new bubbles form in turn. No new nucleation sites were observed after the first 10 min post decompression start so bubble density did not vary after this point in the experiment. In addition, a competition for dissolved gas between adjacent multiple bubbles was demonstrated in increased delay times as well as slower growth rates for non-isolated bubbles.

1. Introduction

Decompression sickness (DCS) is a pathophysiology caused by gas bubbles which grow in the body during a reduction in ambient pressure (decompression) that can affect divers, astronauts, pilots and compressed air workers [1]. With over 7 million active recreational scuba divers worldwide [2,3] and new evidence for potential long term effects even in recreational divers who never had symptoms [4], it is alarming to note that scuba divers who follow current decompression procedures can still get DCS. Vascular gas bubbles are routinely observed even after asymptomatic SCUBA dives using ultrasound imaging and are considered a key element in the potential development of decompression sickness. The precise formation mechanism and site of these bubbles are still debated [5] and bubble growth from decompression in vivo has not been extensively studied, due in part to imaging difficulties [6].

Previous experiments on decompressed rats [7–10] looked at bubble growth/shrinkage on muscle and fat depending on the gas breathed. However, the main difficulty to date has been that the set-ups do not allow for real time observation of bubble growth during the decompression and tissues/animals have to be taken out of the chamber to be observed. For animals, the difficulty in locating bubbles means that bubbles often have to be injected [10]. For tissues, in addition to the potential problem from dislodgment

* Corresponding author at: Department of Bioengineering, Imperial College London, London, UK. Tel.: (+44) (0)20 75 94 36 64.
** Co-corresponding author at: Department of Chemistry, Aristotle University of Thessaloniki, Thessaloniki, Greece.
E-mail addresses: virginie.papadopoulou07@imperial.ac.uk (V. Papadopoulou), karapant@chem.auth.gr (T.D. Karapantsios).

http://dx.doi.org/10.1016/j.colsurfb.2015.03.027
0927-7765/

of bubbles with movement (opening chamber and taking samples out), the observation is then often done in non-ideal conditions such as waiting for the bubbles to float [11–13].

The first aim of this study is thus to develop a new experimental set-up to allow for the first time real time observation *during* decompression of bubble growth from desorption of inert gases out of solutions on tissue substrates. In order to quantify the different parameters that could influence inception delay times, growth rate, detachment and multiple bubble behavior, this set-up should allow for different gases and liquid compositions, temperature control, as well as optical recording of both bubble density per unit surface and precise bubble growth rate.

Higher subject fat percentage has been demonstrated as a risk factor for higher bubble grades post dive [14,15]. Although not fully understood, adiposity as a risk factor for developing decompression sickness (DCS) has been discussed for decades. It is usually attributed to either nitrogen solubility and diffusion arguments, or fitness-related variability in subjects' ability to cope with bubbles. We hypothesize that, in addition to nitrogen uptake and subject cardiovascular fitness, the hydrophobicity of adipose tissues may facilitate bubble growth during decompression.

The second aim of this study is therefore to investigate the role of the tissue substrate (surface), mainly of fat and muscle ex vivo rabbit tissues since fat and muscle have been used most in newer decompression modeling efforts [16–19], in the decompression induced bubble growth rate and density with nitrogen taken as the inert gas.

2. Material and methods

2.1. Experimental set-up developed

Figs. 1 and 2 show the different components of the set-up which allows for the first time the observation in real time during decompression of the growth rate of selected bubbles, but also bubble density per unit surface area, comparing how these vary for different tissue surfaces, decompression profiles, gas saturated liquid composition and temperature. Two configurations for optical acquisition were optimized to allow for subsequent semi-automated data analysis using image processing techniques: for growth data of individual bubbles maximum magnification and lighting straight from the back of the chamber, and for density data with lesser magnification and acquisition at an angle to look at a number of bubbles per surface area (calibrated with millimeter paper to get field of view precisely). The resolution of the optical system was assessed from calibration against a known thickness wire of 56 μm.

2.2. Experimental procedure

After Ethics Committee approval (59001/536) in accordance to EU Directive 2010/63/EU for animal experiments, ex vivo muscle and fat tissues from rabbits were obtained for the experiments and all animal handling was done by our collaborators in the veterinary school (see acknowledgements). Rabbits (male, 3 months old, $n = 8$) were anaesthetized then euthanized by injection of sodium pentothal and potassium chloride respectively. Excised dorsal subcutaneous white adipose tissue and quadriceps muscle samples were then extracted within 15 min and placed directly in physiological saline. These were stored at 4 °C for preservation and used in the experiments within 48 h. The tissues were covered with nitrogen saturated distilled water and eight decompression experiments performed, from 3 bar to 0 bar, at a decompression rate of 1 bar/min as described thereafter.

The following description relates to our particular experiment, however different gases, liquids, tissues and temperatures could be used with this set-up. A compressed nitrogen tank is used to saturate distilled water at just above 3 bar (taking reference of 0 bar

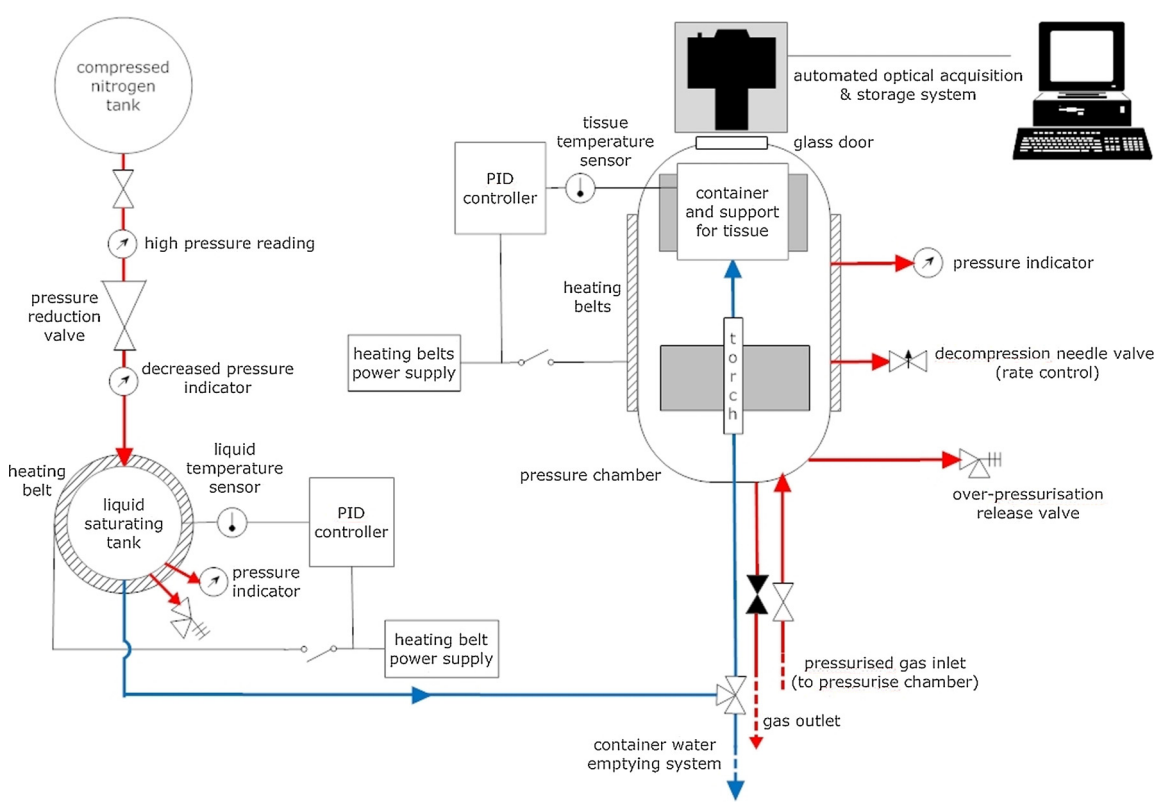

Fig. 1. Top view schematic of experimental set-up, showing liquid (in blue) and gas (in red) pressure flow systems. (For interpretation of the references to color in this figure legend, the reader is referred to the web version of this article.)

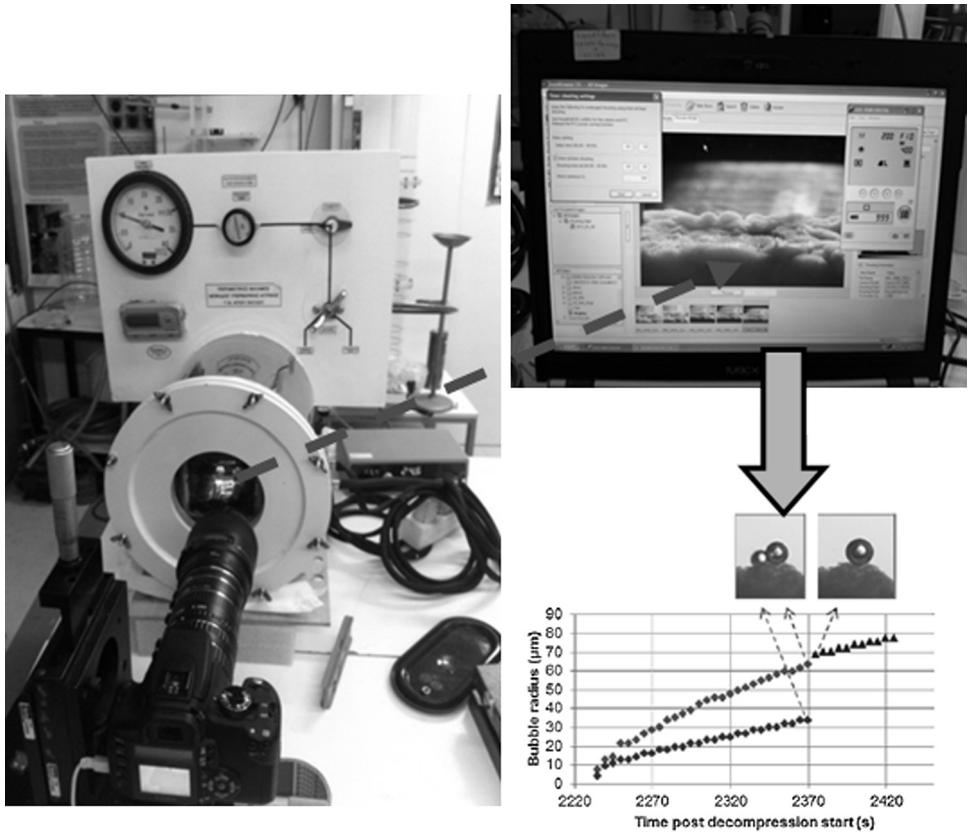

Fig. 2. Photograph showing the optical acquisition system and the temperature controlled small pressure chamber, as well as an example result.

atmospheric pressure) in the water liquid saturation tank which is temperature controlled with a PID device at 25 °C. The tissue is carefully placed in the glass container in the chamber, after switching on the dive torch used for back lighting the tissue and bubbles in order to get good quality images for image processing thereafter (black bubbles on a light background). The pressure chamber, also temperature controlled using another PID device at 25 °C, is pressurized to 3 bar above atmospheric pressure using compressed air. The liquid saturation tank valve is then opened for the liquid to flow into the pressure chamber through a tube connected to the custom made glass compartment with the ex vivo tissue. The liquid entry valve of the chamber is then closed again once the tissue is covered completely. The camera used for optical acquisition is refocused (water entry changes the refraction) and automatic acquisition every 5 s started to coincide with the start of the decompression, done at a rate of 1 bar/min (equivalent to 10 msw/min) without interruptions from the initial saturation of 3 bar (30 m depth equivalent) to 0 bar (surface pressure) with a needle valve.

2.3. Image processing

A custom MatLab[1] image processing code was written for bubble tracking in successive frames, based upon a Hough transform for circle pattern recognition [20–22]. The program identifies the bubble radii and center positions, tracking those over a time sequence of pictures, then outputs the results in an excel file for analysis. In addition, figures displaying the original picture and overlaying the bubbles centers and radii are also created and saved. The program successfully tracks bubble growth over time. Conflict resolution if multiple radii and/or centers are found, as well as consistency checks, are implemented to ensure correct results are output to the excel file. The main steps of the code are shown in Fig. 3.

The sequence for bubble recognition using the Circular Hough Transform feature extraction is fully automatized. However, in practice it is convenient to have the user select a small range of radii as the algorithm input in order to accelerate the running time of the program which can take tens of minutes when the sequence of picture is long for a search over a wide radius range (over 50 pixels). A simple GUI was therefore created to speed up the process: it asks the user to manually select all the pictures to analyze for a sequence (with possibility to input more than one sequence at a time), displays the first and last pictures for the user to draw the bubble outline and input the time delay between successive pictures (taken 5 s apart in our experiment), and initialize the algorithm from these user inputs (namely region of interest and radius range).

2.4. Theoretical analysis for bubble growth

Gas bubble growth on a substrate due to decompression is a complex physicochemical process. A detailed mathematical formulation is not given here but the key issues of the process are described. The difference between the instantaneous gas concentration in the liquid phase from the gas solubility (equilibrium, i.e. maximum, dissolved gas concentration) at the specific thermodynamic conditions (temperature, pressure) is the driving force for bubble growth. The motion of the gas–liquid interface as a bubble grows induces motion to the surrounding liquid. Gas has to be transferred inside the liquid flow field by diffusion and convection in order to reach the bubble surface. The pressure in the bubble increases with respect to the liquid pressure by the Laplace pressure term (surface tension effect) and the pressure needed

[1] All data processing was performed off-line using a commercial software package (MATLAB 7.13, The MathWorks Inc., Natick, MA, 2011).

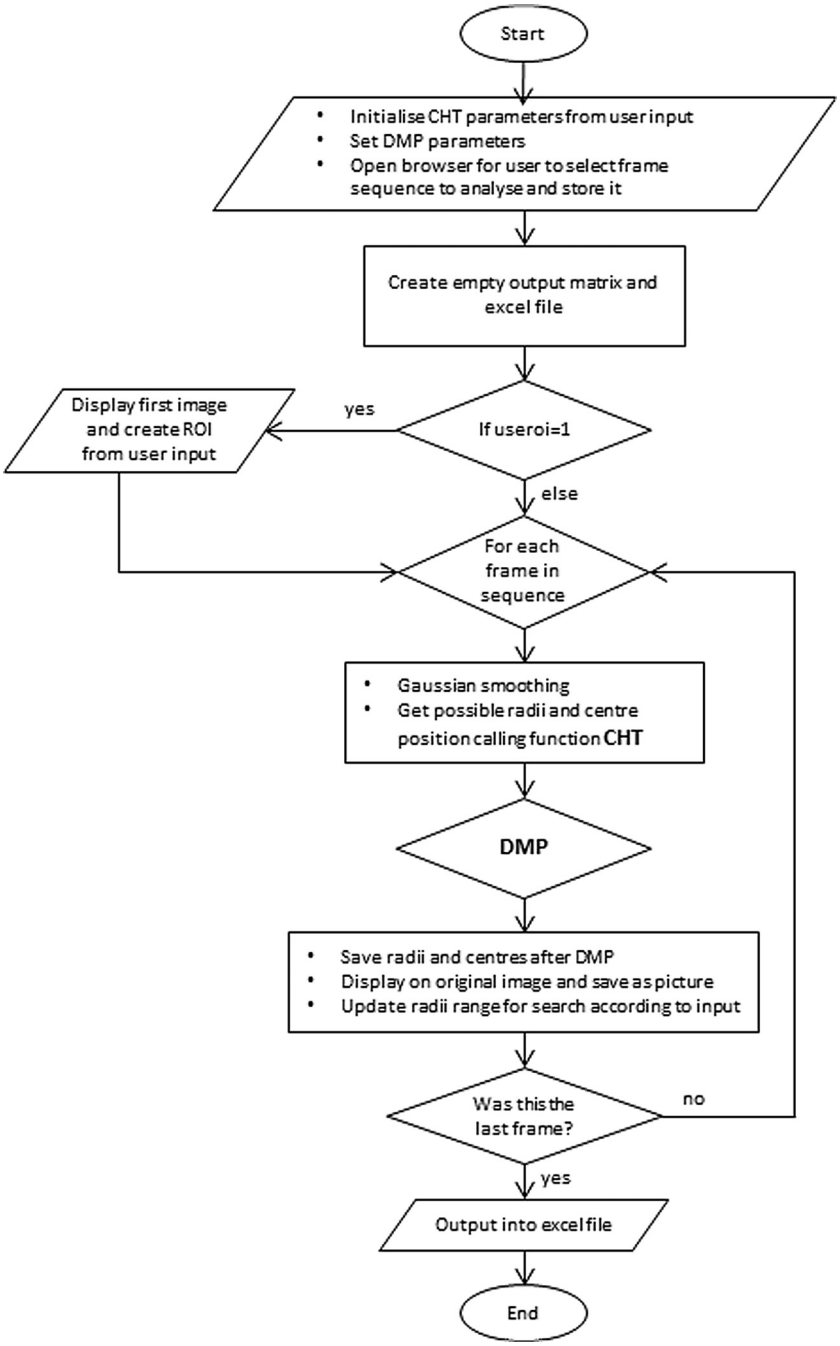

Fig. 3. Flowchart of analysis code in MatLab. CHT: circular Hough transform; DMP: decision making process to keep only one radius and center per bubble if multiple choices given in CHT output, by taking into account the previous frame output for centers and/or ROI and/or radius value (depending on user choice for DMP input parameters).

to support liquid motion (as described by the Rayleigh–Plesset equation [23]). The shape of the bubble is spherical for diameters less than 1 mm [23] (more specifically spherical segments for non-zero contact angle). Finally, the bubble interior consists of desorbed gas and vapor (to account for vapor pressure). In addition to the above general considerations, a total balance of the dissolved gas is needed for the particular experimental set up used here since gas is consumed gradually due to creation and growth of bubbles.

In principle, a bubble growth mathematical model must account for all the above issues. Fortunately a great deal of simplification is possible under the present experimental conditions:

(i) The experiments showed bubble growth rates of the order of few micrometers per second. For such growth rates the overpressure needed to keep the liquid motion is insignificant and the bubble pressure is simply the sum of the ambient and the Laplace pressure [24].

(ii) The water vapor pressure at the experiment temperature of 25 °C is less than 0.03 bar which means that the water vapor molar fraction in the bubble is less that 3% so it can be safely ignored. The bubbles can be assumed to consist only of gas.

(iii) The measured contact angles are relatively small so the bubbles can be assumed to be approximately whole spheres (and not spherical segments).

(iv) The relative significance of convection and diffusion of the dissolved gas on bubble growth is determined through the so called Foaming number [25]. The Foaming number is given as $(C - C_{eq})/\rho_g$ where C is the initial dissolved gas concentration

(at 4 atm), C_{eq} the equilibrium dissolved gas concentration (gas solubility) at the final pressure (1 atm) and ρ_g the gas concentration in gas phase at the final pressure. These assumptions are possible due to the fact that the decompression time is small compared to the experiment time and it can be assumed that the bubble growths occur after the decompression is over, under a constant pressure of 1 atm.

(v) A global balance of the dissolved gas considering the nucleation rate, the bubble size and the dissolved gas concentration reveals that the reduction of the dissolved gas concentration during the experiment is small and can be neglected (due to large liquid volume so C remains constant during the experiment).

The Foaming number in the present experiment is therefore found to be 0.045. This small value indicates domination of diffusion over convection which means that the latter can be ignored. Discard of convection is a major simplification which disconnects the liquid flow field from the bubble growth problem. The above assumptions may lead to an error of a few percent which is below the resolution capabilities of the experimental technique so there is no point to care to relax them by employing far more complex models.

Solution of the pseudo steady diffusion equation in the liquid domain combined to a bubble gas balance leads to:

$$\left(\rho_g + \frac{4\gamma}{3RR_gT}\right)\frac{dR}{dt} = \frac{\alpha D(C - C_{eq})}{R}, \tag{1}$$

where R is the bubble radius, R_g is the gas constant, t is time, T is temperature, D is gas in liquid diffusivity and γ is the surface tension. A mathematical analysis can show that the effect of surface tension term for bubbles with radius larger than 20 μm is comparable to the resolution of the experimental data so it can be safely ignored leading to:

$$R = \left(\frac{2\alpha D(C - C_{eq})t}{\rho_g}\right)^{1/2}, \tag{2}$$

The parameter α is of particular importance and it is related to the geometry external to the bubble domain (i.e. it results from the solution of the diffusion equation in this domain). Two exact values are $\alpha = \ln(2)$ [26] for bubble growing on a flat substrate and $\alpha = 1$ for bubble growing in infinite liquid domain. In principle, the relative curvature of the substrate can change as bubble grows but this variation is general small so a constant in time α has been assumed. According to the above analysis, the only reason for observing differences in the growth rate is the local geometry of the substrate around the nucleation site. There is an exception to the above statement in case of proximity of two nucleation sites (two adjacent bubbles). The concentration field around the bubble diminishes as R/r (r is the radial distance from the bubble) so two bubbles at short distance from each other exhibit reduced growth rates.

2.5. Data fitting and statistical methods

According to the theoretical analysis the bubble radius evolution curve has the form $R = At^{0.5}$. Direct use of the above equation to fit experimental data requires the exact knowledge of the bubble creation (inception) time. This is not possible due to the singular character of the growth equation at $t = 0$ (infinite growth rate) and the experimental finite bubble detection ability. So it is found very fruitful to estimate bubble creation moment by using it as fitting parameter.

Bubble radii over time were fitted with a constrained power law as it is expected [6] that the mass diffusion growth curves should follow the form:

$$R(t) = At^{0.5}, \tag{3a}$$

where R is the bubble radius, t time taken from the inception of the bubble and A is a constant.

The exact inception (time-of-onset of nucleation) time $t = 0$ is not known since there is a resolution limit to the optical set-up, as well as a time delay of 5 s between successive pictures. This inception time, t_0, is therefore extracted from the observed time-dependence of the bubble radius, by re-writing [Eq. (3a)] as:

$$R(t) = A(t - t_0)^{0.5}. \tag{3b}$$

In order to fit growth curves to Eq. (3a) and (3b) and estimate the A coefficients as well as the goodness of fit (G), the exact bubble inception time t_0 is therefore estimated by squaring both sides of Eq. (3b) and fitting a linear equation with constrain $\beta > 0$,

$$y = \alpha \quad t + \beta, \tag{4}$$

where by design $y(t) \equiv R^2(t)$, $A \equiv \sqrt{\alpha}$ and $t_0 \equiv \frac{-\beta}{\alpha}$.

All data is presented as mean ± standard deviation. Statistical comparison tests between the muscle and fat quantities measured were performed with Mann–Whitney U test after negative normality test. Statistical significance levels were set at $p < 0.05$ (*), $p < 0.01$ (**) and $p < 0.001$ (***).

3. Results

An experimental set-up was developed to allow for the observation of bubble growth rate *during* decompression on ex vivo tissue surfaces. A total of 22 experiments were performed without any decompression stop (3 bar to 0 bar at a rate of 1 bar/min): 11 with fat tissue substrate (6 with the camera focused for growth and 5 primarily with the camera focused on density) 11 with muscle tissue substrate (6 with the camera focused for growth and 5 primarily with the camera focused on density). The bubble growth observed from the experiments happen in a cyclic manner from nucleation sites. The phenomenon observed is typical of heterogeneous nucleation where a bubble starts growing from a preferential site (nucleation site) until it finally detaches and floats, then another bubble grows from that same site, etc. in a cyclic manner [27].

With the 12 experiments where the camera was focused for growth sequences, a total of 74 bubble growth sequences were observed (35 on fat tissue substrate of which 20 contained multiple bubbles in the field of view, and 39 on muscle tissue substrate of which 25 contained multiple bubbles in the field of view). There were also 16 sequences of bubbles growing from below camera resolution, 15 sequences observed until bubble detachment and a total of 23 sequences with good enough quality on the substrate to extract contact lines and contact angles.

3.1. System evaluation

The experimental set-up allows the accurate and sensitive optical recording of bubble growth and density on tissue surface area measurement (field of view of 6.38 mm × 4.25 mm, with a resolution of 1.75 μm) during hyperbaric decompression. The semi-automated analysis code is able to track bubble growth sequences successfully (with a maximum associated radius error of ±2 μm) and implementation time is significantly reduced from the user initialization of the radii range.

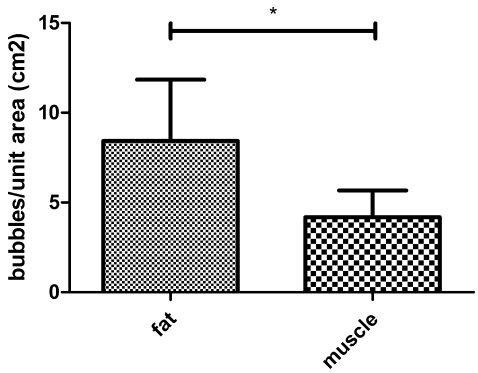

Fig. 4. Bubble density comparison between fat ($n = 11$) and muscle ($n = 11$) tissue substrates.

3.2. Bubble density

A significant difference in density of bubbles formed on muscle and fat was found, respectively 4.2 ± 1.5 and $8.4 \pm 3.4\,\text{cm}^{-2}$ (Fig. 4), with significance set at $p < 0.05$. The densities were measured at 30 min post decompression start since the cyclic growth observed means no new nucleation sites are observed in practice after about 15 min post decompression start, and the bubbles per surface area stay roughly constant throughout the experiment after that point (minus bubble floating before new bubble appears for some seconds). It should be noted that the nucleation sites are not equally distributed on the tissue surfaces and some areas have more densely packed bubbles than others.

3.3. Growth rate

All bubbles observed growing from below resolution were fitted to a constrained power law, as it is expected [4] that the mass diffusion growth curves should follow the form: $R(t) = At^{0.5}$, where R is the bubble radius, t time taken from the inception of the bubble and A is a constant. Goodness of fit was very good (G coefficients for muscle and fat were 0.95 ± 0.076 and 0.97 ± 0.036 respectively), and no significant difference between the two tissues was found for the A coefficients (9.8 ± 4.1 and 9.0 ± 1.2 respectively for muscle and fat tissue substrates).

Taking *all single* bubbles observed, not only the ones observed from below resolution size, fitting with the radii with the expected mass diffusion growth curves showed a goodness of fit such that G coefficients for muscle and fat were 0.98 ± 0.02 and 0.97 ± 0.03 respectively, and again no significant difference between the two tissues was found for the A coefficients (11.0 ± 8.57 and 12.4 ± 8.73 respectively for muscle and fat tissue substrates). The superimposed bubble growth curves for both muscle and fat tissue substrates from calculated bubble inception time are shown in Fig. 5.

Using the experimental conditions and the physical parameters of nitrogen, the value of A for the present experiments is found to be $12.6\alpha^{0.5}\ \mu\text{m/s}^{0.5}$. Considering the typical geometry dependent range of α (0.7–1), it is clear that this value is very close to the average experimental values. The theory predicts the magnitude of A and the small difference between its value for different substrate geometries. On the other hand, the experimental scatter in A values cannot be explained at present. Arguments regarding the local consumption of dissolved gas (in contrast to the global consumption which has been deemed insignificant) seem plausible to justify a range of A values instead of a single value. Interestingly, modifications of the nucleating sites by geometric abrasions on a controlled surface were shown to affect bubble detachment size as well as produce deviations from Scriven behavior [28].

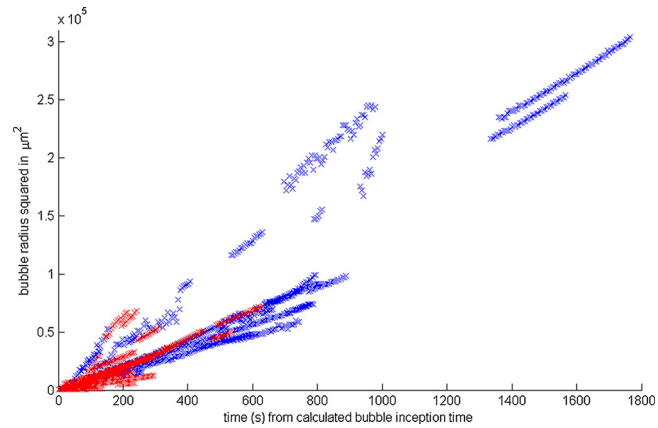

Fig. 5. Superimposed muscle (red) and fat (blue) bubble growth data. (For interpretation of the references to color in this figure legend, the reader is referred to the web version of this article.)

3.4. Detachment size and delay times in cyclic growth

Cyclic bubble growth delay times (after the first nucleation delay) are not found significantly different: 5 ± 3 s for fat versus 7 ± 5 s for muscle. Detachment sizes (last size before bubbles float) are significantly different: $439 \pm 52\ \mu\text{m}$ for fat versus $213 \pm 52\ \mu\text{m}$ for muscle (Fig. 6), possibly due to the differences in geometric and/or wetting properties of the substrates.

The observation that detachment size for bubbles on muscle tissue substrate is significantly less than for fat tissue (Fig. 6) is also reflected in Fig. 5 showing more smaller bubbles compared to bigger ones on muscle.

3.5. Contact lines and contact angles

Image processing results for contact line and contact angles are shown in Fig. 7.

In the five cases where the bubble subsequently detaches the contact line shrinks dramatically during that sequence as expected. Excluding these however, for each individual sequence no clear trend is visible in terms of evolution of the contact line and contact angle. Since the rate of bubble growth is slow, this could be due to the time of observation of each sequence combined to the fact that the quantities discussed here are the *apparent* contact lines and angles (with a higher associated measurement error, possibly due to microstructures or uneven tissue surface). A more representative measurement would therefore be to superimpose all contact angles and contact lines measured.

Mean contact angle and contact line distance evolution over time from calculated bubble inception time (in the same manner as what was presented for Fig. 5) were thus plotted and slopes of the evolution fitted linearly extracted ($n = 23$). The mean contact angle was shown to decrease over the bubble growth time ($y = -0.014t + 35$, $G = 0.54$), whereas the contact line trend was shown positive ($y = +0.04t + 116$) but with only $G = 0.1$ making this a weak trend.

For a gas bubble growing from a substrate's cavity, it is expected that the contact angles will shrink as the bubble grows outward if it remains spherical which is the case in our experiment. The question remains as to whether the contact line stays anchored at the mouth of the cavity during growth. All but three of our data regarding CL/CA come from the fat tissue substrate (no difference was immediately obvious between the muscle and fat ones, however not enough data is available to conclude) and fat is supposed to be hydrophobic from the literature [13,29]. It is expected that a bubble growing on a hydrophobic surface will free

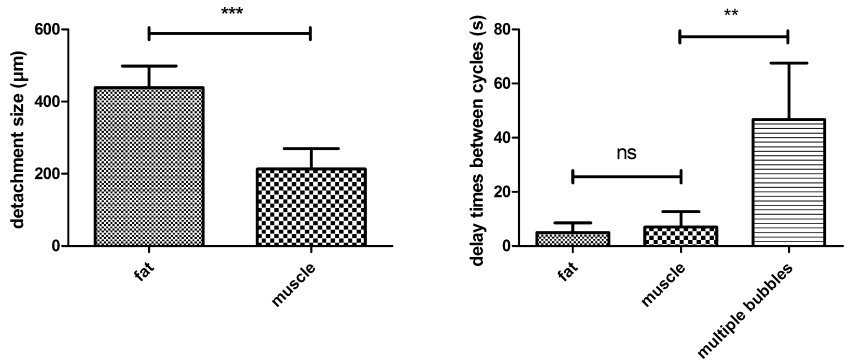

Fig. 6. Bubble radius at detachment (left, fat $n = 8$, muscle $n = 7$) and delay times between bubbles growing from same nucleation site (right, fat $n = 7$, muscle $n = 6$ and multiple $n = 6$), for muscle and fat tissue substrates.

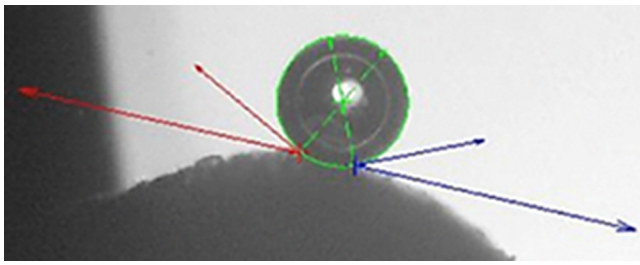

Fig. 7. Example bubble tracking result from custom MatLab code.

itself from the cavity's mouth and thus its contact line would be shown to increase over its growth time [30]. This is still plausible from our results given the positive slope found for the contact line over bubble growth time, however the weak correlation ($G = 0.1$) together with the fact that the contact angles measured on fat are consistently well below 90° point to our substrate not being particularly hydrophobic in this case.

3.6. *Multiple bubbles: competition for dissolved gas and coalescence behavior*

A competition for dissolved gas between adjacent bubbles is demonstrated in increased delay times in cyclic growths from the same nucleation site once a bubble has detached (Fig. 6), as well as slower growth rates for non-isolated bubbles. The growth rate of bubbles growing close to each other departs for the constrained parabolic law fitting, which is evidence for dissolved gas competition amongst multiple bubbles growing in close proximity. For multiple adjacent bubbles, the G coefficients for muscle and fat were indeed significantly worse than for single bubbles at 0.84 ± 0.20 and 0.92 ± 0.08 respectively. Interestingly, in almost all cases one bubble of the adjacent multiples seemed to dominate in the competition for dissolved gas from the liquid as demonstrated by a G closer to the single bubbles' and the rest of the bubbles showed significant departures from the expected mass diffusion growth curves (with G as low as 0.38).

4. Discussion

Results from this first study indicate that, by effectively decoupling the effects from tissue gas absorbance rate and tissue surface, it is possible to ascertain that tissue surface also plays a role in the difference observed between fat and muscle bubbles and that this is not solely due to fat tissues absorbing more inert gas as is often quoted in historical physiological papers. The key novelty in this work, however, remains the development of an experimental set-up, as well as specific data processing software, for studying decompression induced bubble growth rate and density on ex vivo tissue surfaces that we consider as "dead" (not metabolizing), with *real-time* optical imaging acquisition and full temperature control, down to μm resolution. This method can be directly extended to the study of different pressure profiles, gas mixtures, tissues or other substrates, temperature regulations and liquid compositions, etc. In addition, in vitro or in vivo experiments in the small decompression chamber could also be considered with the same imaging and data processing capabilities as described presently.

The use of a circular Hough transform based algorithm has the clear advantage of complete robustness if the bubble grows slightly out of the focus plane field, as the principal radius component is picked up through an ordered voting process. In addition, lighting the bubbles from the back permits to focus the camera in the exact center of the bubble when first observed as they appear black with a fine white inner circle due to the light set-up chosen. Combined to the facts that the optical acquisition is done automatically from the outside of the chamber and the temperature controlled throughout the experiment, this allows for the most precision of the measurements as the set-up is properly sealed throughout the measurements with samples not even touched (and indeed anecdotally on touching the small decompression chamber without even attempting to open it bubbles were seen to immediately start to float).

For multiple bubbles growing in close proximity, it was shown that the G goodness of fit coefficient for parabolic growth is on average less good than for single bubbles. Interestingly the standard deviation is also significantly increased. This is due to the fact that in most cases of multiple bubble growths there is one bubble that dominates (with higher R^2 almost comparable to single bubbles) and the other growing significantly slower. This competition for dissolved gas is also demonstrated in the significant bigger delay times between successive bubble cycles growing from the same cavity when multiple bubbles are present (Fig. 6).

If this competition for dissolved gas which has been demonstrated for instance in heat transfer bubble growth in microgravity experiments [31], from the liquid is correct, it is expected that the average G coefficient for multiple bubbles' growth fitting will drop as the distance between two adjacent bubbles decreases or as the number of adjacent bubbles increases. In addition, above a certain distance threshold between bubbles it is expected that the deviation from single bubble behavior will be negligible.

As a very preliminary test for this hypothesis and as a means to generate a hypothesis for further validation studies, taking only the cases where there are only two adjacent bubbles and both are in focus, Fig. 8 shows the trend for the G coefficient against the inverse of the distance between bubble centers in μm. However, the scarcity of available data does not permit to conclude solidly

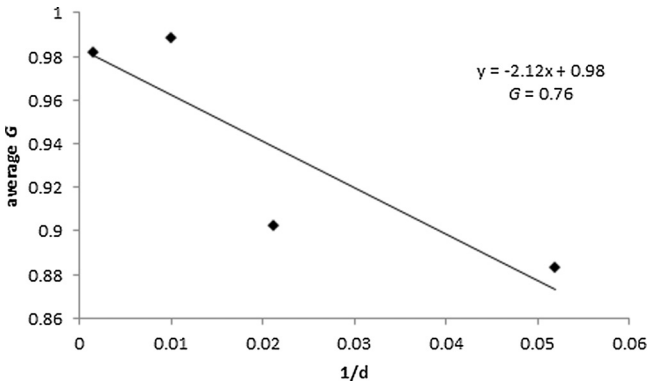

Fig. 8. Inverse relation between distance between two adjacent bubbles and their average *G* coefficient.

on this yet and more observations are needed. This is difficult in practice as the position of appearance of the bubbles with respect to the focusing and field of view of the camera is luck and in our experiments, despite having hundreds of bubble sequences only four cases with only two bubbles and both in focus are recorded. Nevertheless, from this preliminary analysis shown in Fig. 8, it is expected that above around 100 μm distance between the centers of the bubbles then the results will be comparable to single growth bubbles where competition for dissolved gas is negligible.

The multiple bubble behavior also differs between fat and muscle tissue substrates, with bubbles on muscle growing until merging and the dominant bubble then suddenly increasing its radius (such the total volume of the merged bubble corresponds to the sum of volumes of the previous bubbles), whereas multiple bubbles on fat grow until they touch each other and coalesce without merging. This was observed in all bubbles seen to grow to the point where they touched each other. In both cases a translational motion (as in [32]) of the bubbles toward each other is often observed with the slower growing bubble moving preferably toward the dominant one.

Initial nucleation delays for the different tissue substrates can be extracted from the bubble density observations, reflecting the number of nucleation sites, the growth rate, detachment size, as well as delay between bubble cycles information. Looking at the bubbles which are first generation cycles only, the initial distribution of delay times for fat is found to be 180 ± 106 s post decompression start and for muscle 155 ± 59 s post decompression start. This approach, together with the different multiple bubble behavior from different tissues, could be used to feed initial parameters and strategies for decompression models in the future.

5. Conclusions

In conclusion, we describe an experimental set up developed for recording bubbles growth rates on tissue surfaces from gas saturated solutions during a reduction of ambient pressure (decompression), as well as bubble density per tissue area. Although the experiment reported here treats of the case of air saturated distilled water and ex vivo rabbit muscle and fat tissues from 3 to 0 bar decompression at 1 bar/min, this can be extended to other liquid or gas properties and composition, temperatures, decompression profile and nucleation site (tissue surface structure and hydrophobicity).

Muscle and fat tissues from rabbits show significantly different bubble densities with the same decompression profile (3 to 0 bar) but similar growth rates once the bubble has reached a critical size. Heterogeneous nucleation is observed from preferential sites on the tissue substrate, where the bubbles grow, detach and a new bubble forms from the same site in turn. Bubble density, the number of bubbles per unit area (measured at 30 min post decompression start), is found significantly different between the two tissue types with more sites on fat observed. Cyclic bubble growth delay times (after the first nucleation delay) are not found significantly different: 5 ± 3 s for fat versus 7 ± 5 s for fat, nor are the initial delay distributions. Detachment sizes (last size before bubbles float) are significantly different: 439 ± 52 μm for fat versus 213 ± 52 μm for muscle. Finally, a competition for dissolved gas between adjacent bubbles is demonstrated in increased subsequent delay times as well as slower growth rates for non-isolated bubbles.

The role of the tissue substrate, decoupled from the absorption of gas with this new experimental set-up, is therefore demonstrated to also play a role in bubble growth, merging/non-merging behavior, as well as detachment from decompression.

Authors contribution

TDK, TM and VP substantially contributed to conception and design of the study. VP and SE substantially contributed to the experimental set-up development and acquisition of data. VP, MK, TDK, RJE, CB and MXT substantially contributed to the analysis code development, data analysis and interpretation of data. VP drafted the article. SE, RJE, TM, CB, MK, MXT, TDK revised the article critically for important intellectual content. All authors approved the final version of the manuscript to be published.

Acknowledgments

This study was supported by the European Network Action COST MP1106 “Smart and green interfaces – from single bubbles and drops to industrial, environmental and biomedical applications” and the PHYPODE project, financed by the European Union under a Marie Curie Initial Training Network Program (EU-FP7-ITN-264816).

In addition, the authors would like to thank both Dr. Kelly Pavlidou and Prof. Ioannis Savvas of the Veterinary School for their advice and handling of animal tissues.

Appendix A. Supplementary data

Supplementary data associated with this article can be found, in the online version, at http://dx.doi.org/10.1016/j.colsurfb.2015.03.027.

References

[1] R.D. Vann, F.K. Butler, S.J. Mitchell, R.E. Moon, Decompression illness, Lancet 377 (2011) 153–164.
[2] PADI, Professional Association of Diving Instructors (PADI) Worldwide Certification History from 1967 to 2006. Available at http://www.padi.com/padi/en/footerlinks/certhistorynum.aspx (accessed 11.02.12).
[3] R.D. Vann, J.J. Freiberger, J.L. Caruso, Divers Alert Network Report on Decompression Illness, Diving Fatalities and Project Dive Exploration: 2005 edition (based on 2003 data), DAN Technical REPORT, 2005.
[4] W. Hemelryck, P. Germonpré, V. Papadopoulou, M. Rozloznik, C. Balestra, Long term effects of recreational SCUBA diving on higher cognitive function, Scand. J. Med. Sci. Sports 24 (2014) 928–934.
[5] V. Papadopoulou, R.J. Eckersley, C. Balestra, T.D. Karapantsios, M.X. Tang, A critical review of physiological bubble formation in hyperbaric decompression, Adv. Colloid Interface 191 (2013) 22–30.
[6] V. Papadopoulou, M.X. Tang, C. Balestra, R.J. Eckersley, T.D. Karapantsios, Circulatory bubble dynamics: from physical to biological aspects, Adv. Colloid Interface 206 (2014) 239–249.
[7] O. Hyldegaard, M. Moller, J. Madsen, Protective effect of oxygen and heliox breathing during development of spinal decompression-sickness, Undersea Hyperb. Med. Soc. 21 (1994) 115–128.
[8] O. Hyldegaard, J. Madsen, Effect of air, heliox, and oxygen breathing on air bubbles in aqueous tissues in the rat, Undersea Hyperb. Med. Soc. 21 (1994) 413–424.

[9] O. Hyldegaard, J. Madsen, Effect of hypobaric air, oxygen, heliox (50:50), or heliox (80:20) breathing on air bubbles in adipose tissue, J. Appl. Physiol. 103 (2007) 757–762.
[10] O. Hyldegaard, M. Moller, J. Madsen, Effect of He–O_2, O_2, and N_2O–O_2 breathing on injected bubbles in spinal white matter, Undersea Biomed. Res. 18 (1991) 361–371.
[11] R. Arieli, A. Marmur, Decompression sickness bubbles: are gas micronuclei formed on a flat hydrophobic surface? Respir. Physiol. Neurobiol. 177 (2011) 19–23.
[12] R. Arieli, A. Marmur, Dynamics of gas micronuclei formed on a flat hydrophobic surface, the predecessors of decompression bubbles, Respir. Physiol. Neurobiol. 185 (2013) 647–652.
[13] R. Arieli, A. Marmur, Evolution of bubbles from gas micronuclei formed on the luminal aspect of ovine large blood vessels, Respir. Physiol. Neurobiol. 188 (2013) 49–55.
[14] D. Carturan, A. Boussuges, P. Vanuxem, A. Bar-Hen, H. Burnet, B. Gardette, Ascent rate, age, maximal oxygen uptake, adiposity, and circulating venous bubbles after diving, J. Appl. Physiol. (1985) 93 (2002) 1349–1356.
[15] D. Carturan, A. Boussuges, H. Burnet, J. Fondarai, P. Vanuxem, B. Gardette, Circulating venous bubbles in recreational diving: relationships with age, weight, maximal oxygen uptake and body fat percentage, Int. J. Sports Med. 20 (1999) 410–414.
[16] C.R. Gutvik, A.O. Brubakk, A dynamic two-phase model for vascular bubble formation during decompression of divers, IEEE Trans. Biomed. Eng. 56 (2009) 884–889.
[17] C.R. Gutvik, R.G. Dunford, Z. Dujic, A.O. Brubakk, Parameter estimation of the Copernicus decompression model with venous gas emboli in human divers, Med. Biol. Eng. Comput. 48 (2010) 625–636.
[18] C. Acott, D. Doolette, Simulations of near-drowning and decompression sickness: a preliminary study, South Pacif. Underwater Med. Soc. J. 32 (1) (2002).
[19] J.-E. Blatteau, J. Hugon, E. Gempp, O. Castagna, C. Pény, N. Vallée, Oxygen breathing or recompression during decompression from nitrox dives with a rebreather: effects on intravascular bubble burden and ramifications for decompression profiles, Eur. J. Appl. Physiol. 112 (2012) 2257–2265.
[20] E.R. Davies, A modified Hough scheme for general circle location, Pattern Recogn. Lett. 7 (1988) 37–43.
[21] C. Kimme, D. Ballard, J. Sklansky, Finding circles by an array of accumulators, Commun. ACM 18 (1975) 120–122.
[22] H. Li, M.A. Lavin, R.J. Le Master, Fast Hough transform: a hierarchical approach, Comp. Vis. Graphics Image Process. 36 (1986) 139–161.
[23] L.G. Leal, Advanced Transport Phenomena: Fluid Mechanics and Convective Transport Properties, Cambridge University Press, Cambridge, 2007.
[24] N. Divinis, T.D. Karapantsios, M. Kostoglou, C.S. Panoutsos, V. Bontozoglou, A.C. Michels, M.C. Sneep, R. De Bruijn, H. Lotz, Bubbles growing in supersaturated solutions at reduced gravity, AIChE J. 50 (2004) 2369–2382.
[25] N. Divinis, T.D. Karapantsios, R. de Bruijn, M. Kostoglou, V. Bontozoglou, J.C. Legros, Bubble dynamics during degassing of liquids at microgravity conditions, AIChE J. 52 (2006) 3029–3040.
[26] W.M. Buehl, J.W. Westwater, Bubble growth by dissolution: influence of contact angle, AIChE J. 12 (1966) 571–576.
[27] S.F. Jones, K.P. Galvin, G.M. Evans, G.J. Jameson, Carbonated water: the physics of the cycle of bubble production, Chem. Eng. Sci. 53 (1998) 169–173.
[28] G.S. Barker, B. Jefferson, S.J. Judd, The control of bubble size in carbonated beverages, Chem. Eng. Sci. 57 (2002) 565–573.
[29] R. Arieli, Was the appearance of surfactants in air breathing vertebrates ultimately the cause of decompression sickness and autoimmune disease? Respir. Physiol. Neurobiol. 206c (2015) 15–18.
[30] C.G.J. Bisperink, A. Prins, Bubble-growth in carbonated liquids, Colloids Surf. A 85 (1994) 237–253.
[31] T.D. Karapantsios, M. Kostoglou, N. Divinis, V. Bontozoglou, Nucleation, growth and detachment of neighboring bubbles over miniature heaters, Chem. Eng. Sci. 63 (2008) 3438–3448.
[32] N. Divinis, T.D. Karapantsios, R. de Bruyn, M. Kostoglou, V. Bontozoglou, J.C. Legros, Lateral motion and interaction of gas bubbles growing over spherical and plate heaters, Microgr. Sci. Technol. 18 (2006) 204–209.